

360VOTS: Visual Object Tracking and Segmentation in Omnidirectional Videos

Yinzhe Xu, Huajian Huang*, Yingshu Chen and Sai-Kit Yeung

Homepage: <https://360vots.hkustvgd.com/>

Abstract—Visual object tracking and segmentation in omnidirectional videos are challenging due to the wide field-of-view and large spherical distortion brought by 360° images. To alleviate these problems, we introduce a novel representation, extended bounding field-of-view (eBFoV), for target localization and use it as the foundation of a general 360 tracking framework which is applicable for both omnidirectional visual object tracking and segmentation tasks. Building upon our previous work on omnidirectional visual object tracking (360VOT), we propose a comprehensive dataset and benchmark that incorporates a new component called omnidirectional video object segmentation (360VOS). The 360VOS dataset includes 290 sequences accompanied by dense pixel-wise masks and covers a broader range of target categories. To support both the development and evaluation of algorithms in this domain, we divide the dataset into a training subset with 170 sequences and a testing subset with 120 sequences. Furthermore, we tailor evaluation metrics for both omnidirectional tracking and segmentation to ensure rigorous assessment. Through extensive experiments, we benchmark state-of-the-art approaches and demonstrate the effectiveness of our proposed 360 tracking framework and training dataset.

Index Terms—Dataset, omnidirectional vision, visual object tracking, video object segmentation

I. INTRODUCTION

VISUAL object tracking (VOT) and video object segmentation (VOS) are two essential tasks in computer vision for spatially and temporally localizing target objects in video sequences. A robust and precise approach is demanded in various applications such as video analysis, human-machine interaction, and intelligent robots. While both VOT and VOS are integral to understanding object dynamics in videos, their fundamental differences are in the level of localization granularity. VOT approaches typically utilize the bounding box to represent the target position and rough size. In contrast, VOS approaches seek to provide pixel-wise localization of the object’s silhouette frame-by-frame. In the last decade, a remarkable development can be seen in these tasks with the flourish of excellent trackers like [1]–[5] in VOT and [6]–[10] in VOS, as well as various benchmarks including [11]–[15] for VOT and [16]–[19] for VOS. Whereas most existing research

focuses on perspective scenarios, there is little attention paid to object tracking and segmentation in the omnidirectional view.

Omnidirectional object tracking and segmentation employs a 360° camera to track the target object. With its omnidirectional field-of-view (FoV), a 360° camera offers continuous observation of the target over a longer period, minimizing the out-of-view issue. This advantage is crucial for intelligent agents to achieve stable, long-term tracking and perception. In general, an ideal spherical camera model is used to describe the projection relationship of a 360° camera. The 360° image is widely represented by equirectangular projection (ERP) [20], which has two main features: 1) crossing the image border and 2) extreme distortion as the latitude increases. Moreover, due to inherent limitations or manufacturing defects of the camera, the 360° image may suffer from stitching artifacts that would blur, break, or duplicate the shape of objects. Meanwhile, omnidirectional FoV means it is inevitable to capture the photographers. They would distract and occlude the targets. These phenomena are illustrated in Figure 1. Eventually, they bring new challenges to perform object tracking and segmentation in 360° videos.

To tackle these challenges, we first explore a new representation in omnidirectional tracking that utilizes extended bounding field-of-view (eBFoV) for precise target localization. Compared to the commonly used bounding box (BBBox), BFoV [21], [22] represents object localization on the unit sphere in an angular fashion. This representation takes the spherical nature of 360° images into account, providing improved constraints for accurately localizing objects and eliminating dependence on image resolution. We therefore can utilize BFoV to extract less-distorted images for target searching. To enable proper handling of objects even when they occupy significant portions of the omnidirectional image, we further extend the BFoV definition and propose eBFoV to accommodate the extraction of search regions. By leveraging the benefits of eBFoV, we propose a general 360 tracking framework that effectively enhances the performance of the conventional local trackers devised for perspective scenes in omnidirectional scenes.

Furthermore, we present 360VOTS, a challenging benchmark dataset to facilitate research and evaluation on omnidirectional tracking and segmentation, including 360VOT [23] and 360VOS datasets. 360VOT provides dense (rotated) BBBox and BFoV annotations of 120 test sequences. Inheriting parts of sequences from the 360VOT dataset, 360VOS incorporates additional 191 sequences and 30 tracking object categories. This results in a large-scale dataset consisting of a total

Yinzhe Xu is with the Division of Integrative Systems and Design. Huajian Huang and Yingshu Chen are with the Department of Computer Science and Engineering (e-mail: hhuangbg, ychengw, yxuck@connect.ust.hk).

Sai-Kit Yeung is with the Division of Integrative Systems and Design, the Department of Computer Science and Engineering, and the Department of Ocean Science (e-mail: saikit@ust.hk).

The Hong Kong University of Science and Technology, Clear Water Bay, Kowloon, Hong Kong

* corresponding author

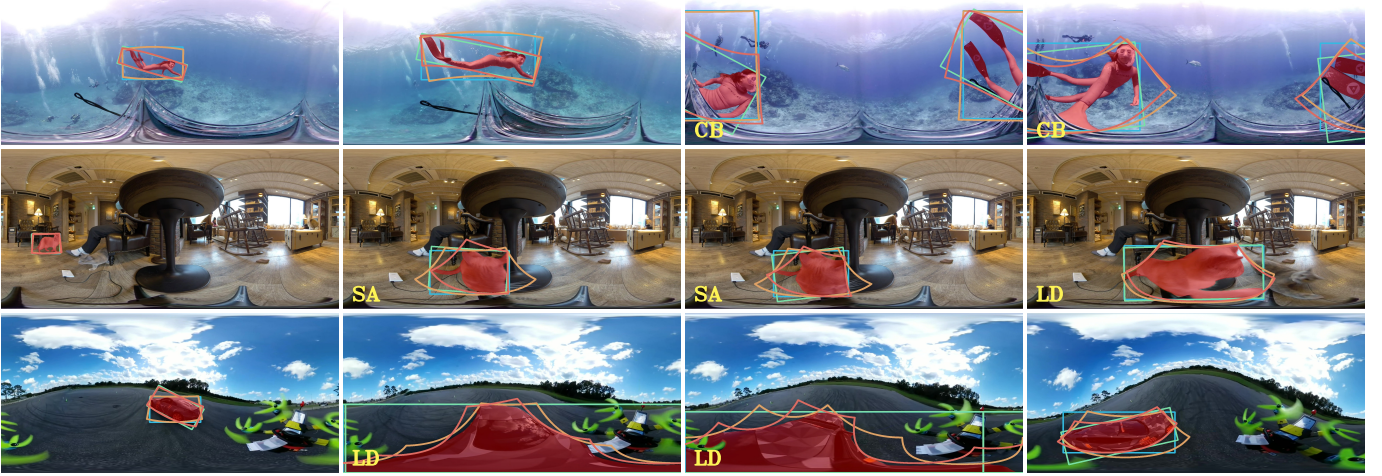


Fig. 1: Example sequences and annotations of 360VOTS benchmark dataset. The target objects in each 360° frame are annotated with **masks** which can be converted into four different representations as ground truth, including bounding box (**BBox**), rotated bounding box (**rBBox**), bounding field-of-view (**BFoV**), and rotated bounding field-of-view (**rBFoV**). 360VOTS brings distinct challenges for tracking and segmentation, i.e., crossing border (CB), large distortion (LD), and stitching artifact (SA).

of 290 sequences in 62 categories. Importantly, 360VOS provides dense pixel-wise annotations as ground truth and assigns 170 sequences as the training set. These pixel-wise annotations are utilized to obtain unbiased (rotated) BBoxes and BFoVs ground truth, ensuring comprehensive evaluation and comparison of different approaches. To accurately evaluate the performance of state-of-the-art (SOTA) approaches on omnidirectional tracking and segmentation, we develop new metrics tailored for 360° images. These metrics encompass dual success, dual (normalized) precision, and angle precision to assess tracking performance, as well as spherical region similarity and spherical contour accuracy to evaluate segmentation performance. Moreover, we exploit the 360VOS training set to retrain the tracker and apply our 360 tracking framework to achieve new SOTA results. With the introduction of new representations, datasets, metrics, and baselines, we believe 360VOTS serves as a vital resource to foster development in omnidirectional visual object tracking and segmentation.

In summary, the contribution of this work includes:

- We explore the new representations for object location in 360° images, as well as a general 360 tracking framework.
- Our proposed 360VOTS is the first benchmark dataset for both omnidirectional visual object tracking and segmentation. We provide densely annotated masks for segmentation and subsequently convert masks into four types of unbiased ground truth for tracking.
- We propose a set of new metrics specifically designed to enable rigorous performance evaluation of omnidirectional tracking and segmentation algorithms.
- We benchmark 20 tracking algorithms and 16 segmentation algorithms on 360VOT and 360VOS respectively, and develop new baselines for future comparisons.

II. RELATED WORK

A. Benchmarks for Visual Object Tracking

With the remarkable development of the visual object tracking community, previous works have proposed numerous

benchmarks in various scenarios.

ALOV300 [24] is a sparse benchmark introducing 152K frames and 16K annotations, while UAVDT [29] focuses on UAV scenarios and has 100 videos. TrackingNet [31] is a large-scale dataset collecting more than 14M frames based on the YT-BB dataset [34]. As YT-BB only provides fine-grained annotations at 1 FPS, they explored a tracker to densify the annotations without further manual refinement. OxUvA [30] targets long-term tracking by constructing 337 video sequences, but each video only has 30 frames annotated.

One of the first dense BBox benchmarks is OTB100 [11] which is extended from OTB50 [35] and has 100 sequences. NUS-PRO [25] takes the feature of occlusion-level annotation and provides 365 sequences, while TC128 [26] researches the chromatic information in visual tracking. UAV123 [12] and DTB70 [27] offer 123 and 70 aerial videos of rigid objects and humans in various scenes. NfS [28] consists of more than 380K frames captured at 240 FPS studying higher frame rate tracking, while LaSOT [14] is a large-scale and category balanced benchmark of premium quality. GOT-10k [15] provides about 1.5M annotations and 84 classes of objects, aiming at generic object tracking. The annual tracking challenge VOT [13] offered 62 sequences and 20K frames in 2022. A more recent benchmark TOTB [32] mainly focuses on transparent object tracking. TREK-150 [33] introduces 150 sequences of tracking in First Person Vision (FPV) with the interaction between the person and the target object.

Differently, our 360VOT focuses on object tracking and explores new representations on omnidirectional videos. A summarized comparison with existing VOT benchmarks is reported in the upper part of Table I.

B. Benchmarks for Video Object Segmentation

There are several benchmarks for video object segmentation proposed in the last decade as described in Table I. FBMS-59 [16] acknowledges the importance of motion information and concentrates on motion segmentation, providing a total of 13,860 frames across 59 sequences. DAVIS [18] is the

TABLE I
Comparison of popular visual object tracking (VOT) and video object segmentation (VOS) benchmarks.

Benchmark	Videos test / train	Total frames	Min frames	Mean frames	Median frames	Max frames	Object classes	Attr.	Annotation	Feature	Year
ALOV300 [24]	314	152K	19	483	276	5,975	64	14	sparse BBox	diverse scenes	2013
OTB100 [11]	100	81K	71	590	393	3,872	16	11	dense BBox	short-term	2015
NUS-PRO [25]	365	135K	146	371	300	5,040	8	12	dense BBox	occlusion-level	2015
TC128 [26]	129	55K	71	429	365	3,872	27	11	dense BBox	color enhanced	2015
UAV123 [12]	123	113K	109	915	882	3,085	9	12	dense BBox	UAV	2016
DTB70 [27]	70	16K	68	225	202	699	29	11	dense BBox	UAV	2016
Nfs [28]	100	383K	169	3,830	2,448	20,665	17	9	dense BBox	high FPS	2017
UAVDT [29]	100	78K	82	778	602	2,969	27	14	sparse BBox	UAV	2017
OxUvA [30]	337	1.55M	900	4,260	2,628	37,440	22	6	sparse BBox	long-term	2018
TrackingNet [31]	511/30K	226K/14M	96/87	441/471	390/480	2,368/690	27	15	sparse BBox	large scale	2018
LaSOT [14]	280/1,120	685K/2,816K	1,000/898	2,448/2,514	2,102/2,023	9,999/11K	85	14	dense BBox	category balance	2018
GOT-10k [15]	420/9,335	56K/1,403K	29/29	127/150	100/101	920/1,481	84	6	dense BBox	generic	2019
TOTB [32]	225	86K	126	381	389	500	15	12	dense BBox	transparent	2021
TREK-150 [33]	150	97K	161	649	484	4,640	34	17	dense BBox	FPV	2021
VOT [13]	62	20K	41	321	242	1,500	37	9	dense BBox	annual	2022
360VOT [23]	120	113K	251	940	775	2,400	32	20	dense (r)BBox & (r)BFoV	360° images	2023
FBMS-59 [16]	30/29	7,306/6,554	19/19	244/226	210/193	800/720	-	-	sparse Mask	moving objects	2014
DAVIS [18]	30/90	2,860/6,208	31/25	70/69	70/70	127/104	376	15	dense Mask	dense annotated	2017
YouTube-VOS [19]	508/3471	70K/470K	36/20	139/135	150/150	180/180	94	-	sparse Mask	comprehensive	2018
LVOS [17]	50/120	30K/65K	257/200	598/544	489/414	2,000/2,280	27	13	dense Mask	long-term	2023
360VOS	120/170	98K/144K	111/62	821/845	684/714	2,400/2,402	62	20	dense Mask	360° images	2024

first dataset designed for video object segmentation (VOS), annotating 376 classes of objects on each frame of 120 short videos. Leveraging the diverse scenarios and photography conditions on YouTube videos, YouTube-VOS [19] introduces a large-scale VOS dataset with more than 540K frames and contains 3471 and 508 sequences as the training set and the test set separately. Each video clip has a duration of 3 to 6 seconds and is annotated every 5 frames. One of the most recent datasets is LVOS [17] which is the first long-term VOS benchmark dataset with an average length of 560 densely labeled frames. In contrast, our 360VOS provides pixel-wise masks of omnidirectional images for both training and testing.

C. Adapting Object Tracking Schemes in Segmentation

To guarantee high tracking speed, the trackers for single object tracking generally crop the image and search for the target in small local regions. The tracking scheme is vital in selecting searching regions and interpreting network predictions over sequences in the inference phase. A compatible tracking inference scheme can enhance tracking performance. For example, DaSiamRPN [36] explored a local-to-global searching strategy for long-term tracking. SiamX [37] proposed an adaptive inference scheme to prevent tracking loss and realized fast target re-localization. Similarly, localizing the target objects is also vital for video object segmentation tasks. Both RTS [38] and SiamMask [39] demonstrated that pixel-wise masks can provide a more accurate estimation of bounding boxes for VOT tasks. Additionally, their tracking schemes improve the robustness of VOS methods and contribute to target localization in long-term videos.

In 360VOS, we take advantage of eBFoV to localize the targets on 360° videos and obtain less-distorted search regions. It allows us to exploit arbitrary local visual trackers, which are trained on normal perspective images to achieve enhanced performance on 360° object tracking and segmentation.

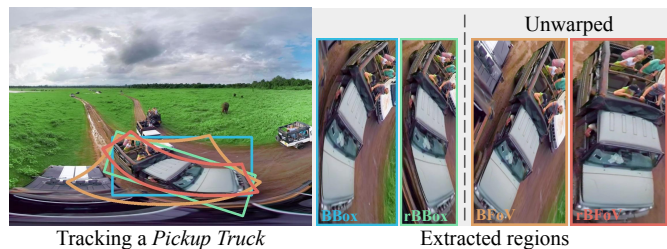


Fig. 2: *Pickup Truck*. The comparison of the bounding regions of different representations on a 360° image. The unwarped images based on BFoV and rBFoV are less distorted.

III. TRACKING ON 360° VIDEO

The 360° video is composed of frames using the most common ERP. Each frame can capture 360° horizontal and 180° vertical field of view. Although omnidirectional FoV avoids out-of-view issues, the target may cross the left and right borders of a 2D image. Additionally, nonlinear projection distortion makes the target largely distorted when they are near the top or bottom of the image, as illustrated in Figure 1. Therefore, a new representation and framework that fits the 360° video for omnidirectional visual tracking is necessary.

A. Representation for the Target Location

The (r)BBox is the most common and simple way to represent the target object's position in perspective images. It is a rectangular area defined by the rectangle around the target object on the image and denoted as $[cx, cy, w, h, \gamma]$, where cx, cy are object center, w, h are width and height. The rotation angle γ of BBox is always zero. However, these representations would become less accurate to properly constrain the target on the 360° image, as depicted in Figure 2. The works [22], [40] for 360° object detection show that the BFoV and rBFoV are more appropriate representations on

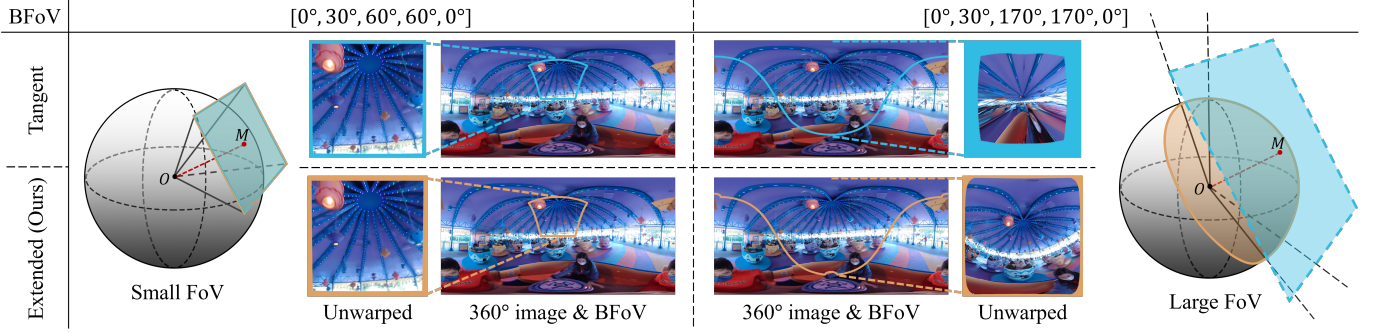


Fig. 3: The boundaries on the 360° images and the corresponding unwarped images of different BFOV definitions. The tangent BFOV is displayed in blue and the extended BFOV is in orange. M on the sphere surface denotes the object center and tangent point. Blue plane with dotted borders represents a larger plane out of space. Best viewed in color.

360° images. Basically, we can use the spherical camera model \mathcal{P} to formulate the mathematical relationship between the 2D image in ERP and a continuous 3D unit sphere [41]. (r)BFOV is then defined as $[clon, clat, \theta, \phi, \gamma]$ where $[clon, clat]$ are the longitude and latitude coordinates of the object center at the spherical coordinate system, θ and ϕ denote the maximum horizontal and vertical field-of-view angles of the object's occupation. The represented region of (r)BFOV on the 360° image is commonly calculated via a tangent plane [22], [40], $T(\theta, \phi) \in \mathbb{R}^3$, and formulated as:

$$I((r)\text{BFOV} | \Omega) = \mathcal{P}(\mathcal{R}_y(clon) \cdot \mathcal{R}_x(clat) \cdot \mathcal{R}_z(\gamma) \cdot \Omega), \quad (1)$$

where,

$$\mathcal{R}_y(clon) = \begin{bmatrix} \cos(clon) & 0 & \sin(clon) \\ 0 & 1 & 0 \\ -\sin(clon) & 0 & \cos(clon) \end{bmatrix}, \quad (2)$$

$$\mathcal{R}_x(clat) = \begin{bmatrix} 1 & 0 & 0 \\ 0 & \cos(clat) & -\sin(clat) \\ 0 & \sin(clat) & \cos(clat) \end{bmatrix}, \quad (3)$$

$$\mathcal{R}_z(\gamma) = \begin{bmatrix} \cos\gamma & -\sin\gamma & 0 \\ \sin\gamma & \cos\gamma & 0 \\ 0 & 0 & 1 \end{bmatrix}, \quad (4)$$

$$\Omega = T = \begin{bmatrix} \mathbf{X} \\ \mathbf{Y} \\ \mathbf{Z} \end{bmatrix} = \begin{bmatrix} -\tan(\theta/2) : \tan(\theta/2) \\ -\tan(\phi/2) : \tan(\phi/2) \\ 1 \end{bmatrix}. \quad (5)$$

The projection function \mathcal{P} to depict the relationship between the 3D camera space $[X, Y, Z]$ and the 2D image space $[u, v]$ is formulated as:

$$\begin{aligned} u &= \left(\frac{lon}{2\pi} + 0.5\right) * W = \arctan(X/Z), \\ v &= \left(-\frac{lat}{\pi} + 0.5\right) * H = \arctan\left(\frac{-Y}{\sqrt{X^2 + Z^2}}\right), \end{aligned} \quad (6)$$

where $-\pi < lon < \pi$ and $-\pi/2 < lat < \pi/2$ denote the longitude and latitude in the spherical coordinate system. W and H are the width and height of the 360° image. The unwarped images based on tangent BFOV are distortion-free under the small FoV, as shown in Figure 2.

However, this definition has a disadvantage on large FoV and cannot represent the region exceeding 180° FoV essentially. With the increasing FoV, the unwarped images from

the tangent planes have drastic distortions, shown in the upper row in Figure 3. This defect limits the application of BFOV on visual object tracking since trackers rely on unwarped images for target searching. To address this problem, we extended the definition of BFOV. When the bounding region involves a large FoV, i.e., larger than 90°, the extended BFOV leverages a spherical surface $S(\theta, \phi) \in \mathbb{R}^3$ instead of a tangent plane to represent the bounding region on the 360° image:

$$S = [\cos(\Phi)\sin(\Theta) \quad -\sin(\Phi) \quad \cos(\Phi)\cos(\Theta)]^T, \quad (7)$$

where $\Phi \in [-\phi/2, \phi/2]$, $\Theta \in [-\theta/2, \theta/2]$. Therefore, the corresponding region of extended (r)BFOV on 360° image is

$$I((r)\text{BFOV} | \Omega), \quad \Omega = \begin{cases} T(\theta, \phi), & \theta < 90^\circ, \phi < 90^\circ \\ S(\theta, \phi), & \text{otherwise} \end{cases}. \quad (8)$$

The comparisons of the boundary on 360° images and corresponding unwarped images based on tangent BFOV and the extended BFOV are shown in Figure 3. For simplicity, BFOV in the following content denotes extended BFOV unless explicitly stated otherwise.

B. 360 Tracking Framework

To conduct omnidirectional tracking and segmentation using an existing local VOT or VOS tracker, we propose a 360 tracking framework, as depicted in Figure 4. The framework leverages extended BFOV to address challenges caused by object crossing-border and large distortion on the 360° image.

Given an initial BFOV or mask, the framework first calculates the corresponding search region I on the 360° image via Eq. 8. Subsequently, by remapping (τ) the 360° image using corresponding pixel coordinates recorded in I , it extracts a less distorted local image for target identification. Within the extracted image, a local visual tracker then infers a (r)BBox or a segmentation mask. Finally, we utilize I to convert the local prediction back to the global bounding region on the 360° image via inverse projection τ^{-1} . For (r)BBox prediction, we calculate the minimum area (rotated) rectangle on the 360° image. For (r)BFOV, we re-project the bounding region's coordinates onto the spherical coordinate system and calculate the maximum bounding FoV. As for the final mask in 360° images, we dilate the reprojected mask to avoid erosion artifacts resulting from inverse projection. To

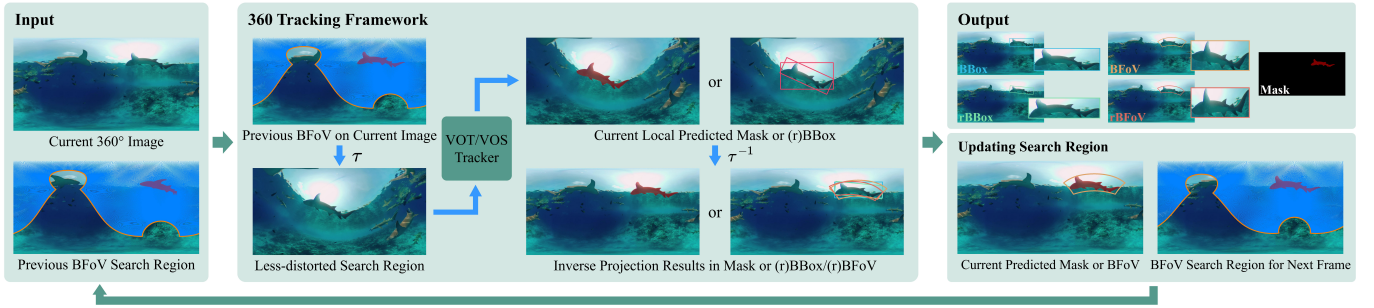


Fig. 4: The 360 tracking framework. The framework focuses on extracting a less-distorted search region to enable precise local visual tracking. The general framework accommodates arbitrary local visual trackers to generate masks or 4 types of representation. τ is the remapping operation to extract the less-distorted search region from the input 360° image, while τ^{-1} is its inverse operation.

maintain continuous tracking, the BFoV search region for the subsequent frame is updated by the current predicted BFoV or mask. In this manner, the search region follows the motions of the target throughout the entire sequence to achieve object tracking and segmentation. It is noted that the framework does not rely on nor affect the network architecture of the tracker, allowing for the adoption of an arbitrary local visual tracker for omnidirectional tracking and segmentation.

IV. BENCHMARK DATASET: 360VOTS

A. Collection and Annotation

The resources of 360° videos in 360VOTS were collected from YouTube or captured using a 360° camera. We ranked and filtered hundreds of candidate videos considering tracking difficulty scale and some additional challenging cases. Videos with additional challenges were assigned a higher priority (i.e. distinguishing targets from other highly comparable objects). Then, videos were further selected and sampled into sequences with a frame number threshold (≤ 2400). The relatively stationary frames were further discarded manually. All selected frames were annotated by an interactive segmentation tool [23]. Considering distribution balance, 120 sequences are finally selected as the 360VOT benchmark and 290 sequences as the 360VOS dataset, sharing 99 sequences for tracking and segmentation benchmarks.

B. Attribute

Each sequence is annotated with a total of 20 different attributes: illumination variation (IV), background clutter (BC), deformable target (DEF), motion blur (MB), camera motion (CM), rotation (ROT), partial occlusion (POC), full occlusion (FOC), aspect ratio change (ARC), scale variation (SV), fast motion (FM), low resolution (LR), high resolution (HR), stitching artifact (SA), crossing border (CB), fast motion on the sphere (FMS), large FoV (LFoV), latitude variation (LV), high latitude (HL) and large distortion (LD).

The detailed meaning of each attribute is described in Table II. Among them, IV, BC, DEF, MB, CM, ROT, POC, and LD attributes are manually labeled, while the others are computed from the annotation results of targets. The distinct features of the 360° image are well represented in 360VOTS: *location variations* (FMS, LFoV, and LV), *external disturbances* (SA and LD) and *special imaging* (CB and HL).

TABLE II

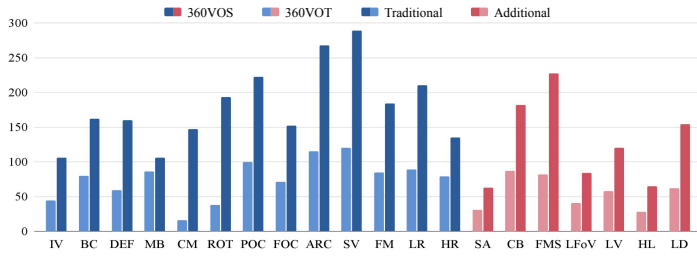
Attribute description. The 360VOTS contains 13 basic attributes widely used in the existing benchmarks, and 7 distinct challenging attributes as described in the last block of the row.

Attr.	Meaning
IV	The target is subject to light variation.
BC	The background has a similar appearance as the target.
DEF	The target deforms during tracking.
MB	The target is blurred due to motion.
CM	The camera has abrupt motion.
ROT	The target rotates related to the frames.
POC	The target is partially occluded.
FOC	The target is fully occluded.
ARC	The ratio of the annotation aspect ratio of the first and the current frame is outside the range [0.5, 2].
SV	The ratio of the annotation area of the first and the current frame is outside the range [0.5, 2].
FM	The motion of the target center between contiguous frames exceeds its own size.
LR	The area of the target annotation is less than 1000 pixels.
HR	The area of the target annotation is larger than 500^2 pixels.
SA	The 360° images have stitching artifacts and they affect the target object.
CB	The target is crossing the border of the frame and partially appears on the other side.
FMS	The motion angle on the spherical surface of the target center is larger than the last BFoV.
LFoV	The vertical or horizontal FoV of the BFoV is larger than 90° .
LV	The range of the latitude of the target center across the video is larger than 50° .
HL	The latitude of the target center is outside the range $[-60^\circ, 60^\circ]$, lying in the “frigid zone”.
LD	The target suffers large distortion due to the equirectangular projection.

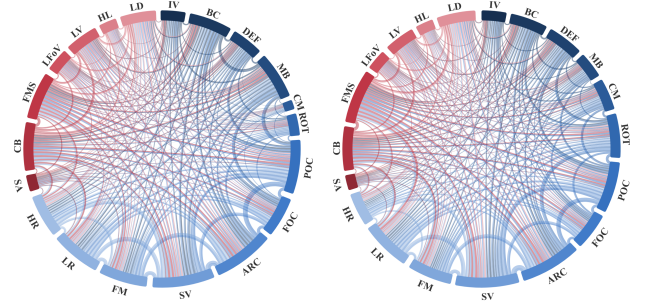
Figure 5 illustrates the comparison between 360VOT and 360VOS in terms of sequence counts and dependencies for each attribute. As shown in Figure 5a, most attributes have similar proportions in 360VOT and 360VOS. In 360VOT, the *scale changes* (ARC and SV) and *motion* (MB and FM) are common challenges illustrated in Figure 5b. By contrast, in 360VOS, the *scale changes* (ARC and SV) remain the predominant features, whereas camera motion (CM) and target rotation (ROT) gain an obvious increase in the number of sequences illustrated in Figure 5c.

C. Dataset Statistics of 360VOTS

360VOTS cover four primary categories of *humans*, *animals*, *rigid objects*, and *human & carrier cases*. As shown in Figure 6, the primary classes are depicted on the branches,



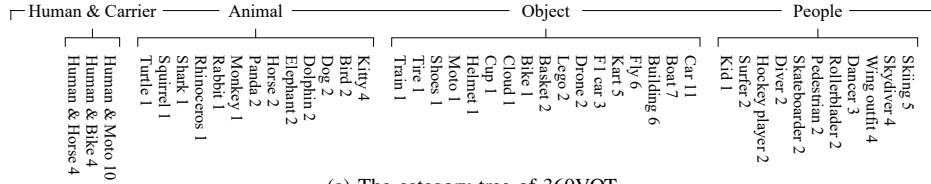
(a) Attribute histograms.



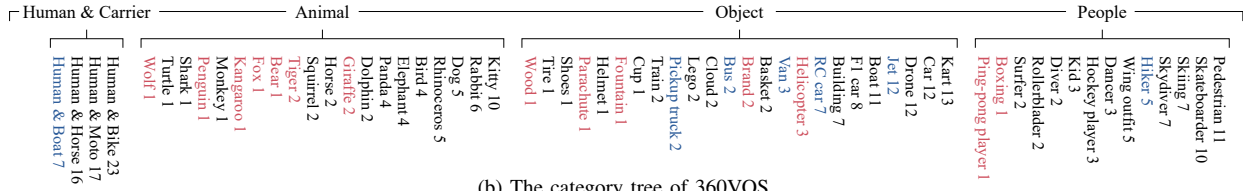
(b) 360VOT dependency wheel.

(c) 360VOS dependency wheel.

Fig. 5: Attribute distributions and dependencies in 360VOTS. The additional introduced attributes are highlighted in red palettes, while the commonly used attributes in existing works are highlighted in blue palettes. The arc lengths on the dependency wheel measure the dominance of the attributes in the dataset. Thicker connection lines indicate a higher frequency of co-presence between attribute pairs, and vice versa.



(a) The category tree of 360VOT.



(b) The category tree of 360VOS.

Fig. 6: The tree maps of the category structures for 360VOTS. Newly introduced classes in 360VOS are highlighted in red, while the classes that have been re-categorized from the original 360VOT are highlighted in blue.

with the leaves denoting the respective sub-classes within each primary class. In the majority of sequences, a single target is annotated across all frames, while up to two components of a single target (e.g. bicyclist and bicycle) are annotated separately in several sequences under the *human & carrier cases* class. Overall, the 120 sequences in the 360VOT dataset are grouped into 32 sub-classes and used for evaluation only. The 360VOS dataset has 62 sub-classes and covers more expansive sequences. In addition, we split the 360VOS dataset into training and test sets with balanced classes of tracking targets, avoiding class bias between the two sets. Eventually, the test set of 360VOS comprises 98,487 annotated frames across 120 sequences and the training set includes 143,634 annotated frames within 170 sequences. As a benchmark suitable for long-term tracking and segmentation evaluation, 360VOS is characterized by an average of 821 frames per sequence in the test set and 845 frames per sequence in the training set, respectively, as reported in Table I.

V. EXPERIMENTS

A. Evaluation Metrics

Evaluation on bounding regions. To conduct the experiments on the tracking results, we use the standard one-pass evaluation (OPE) protocol [11] and measure the success S , precision

P , and normalized precision \bar{P} [31] of the trackers over the test sequences. Success S is computed as the intersection over union (IoU) between the tracking results B^{tr} and the ground truth annotations B^{gt} , where the $B^{tr/gt}$ indicates a (r)BBBox. The trackers are ranked by the area under curve (AUC), which is the average of the success rates corresponding to the sampled thresholds $[0, 1]$. The precision P is computed as the distance between the results C^{tr} and the ground truth centers C^{gt} . The trackers are ranked by the precision rate on the specific threshold (i.e., 20 pixels). The normalized precision \bar{P} is scale-invariant, which normalizes the precision P over the size of the ground truth and then ranks the trackers using the AUC for the \bar{P} between 0 and 0.5. For the perspective image using (r)BBBox, these metrics can be formulated as:

$$S = IoU(B^{gt}, B^{tr}), P = \frac{\|C_{xy}^{gt} - C_{xy}^{tr}\|_2}{\|diag(B^{gt}, B^{tr})(C_{xy}^{gt} - C_{xy}^{tr})\|_2} \quad (9)$$

However, for 360° images, the target predictions may cross the image. To handle this situation and increase the accuracy of BBox evaluation, we introduce dual success S_{dual} and dual precision P_{dual} . Specifically, we shift the B^{gt} to the left and right by W , the width of 360° images, to obtain two temporary ground truth B_l^{gt} and B_r^{gt} . Based on the new ground truth, we then calculate extra success S_l and S_r , and precision P_l and P_r .

using Eq. 9. Finally, S_{dual} and P_{dual} are measured by:

$$S_{dual} = \max\{S_l, S, S_r\}, \quad P_{dual} = \min\{P_l, P, P_r\}. \quad (10)$$

S_{dual} and S , as P_{dual} and P , are the same when the annotation does not cross the image border. Similarly, we can compute the dual normalized precision \bar{P}_{dual} .

Since objects suffer significant non-linear distortion in the polar regions due to the equirectangular projection, the distance between the predicted and ground truth centers may be large on the 2D image but they are adjacent on the spherical surface. It means that dual precision P_{dual} is sensitive for 360° images. Therefore, we propose a new metric P_{angle} , which is measured as the angle precision between the vectors of the ground truth and the tracker results in the spherical coordinate system. The angle precision P_{angle} is formulated as:

$$P_{angle} = \|\mathbf{C}_{lonlat}^{gt} - \mathbf{C}_{lonlat}^{tr}\|_2. \quad (11)$$

The different trackers are ranked with angle precision rate on a threshold, i.e., 3°. Moreover, when target positions are represented by BFoV or rBFoV, we utilize spherical IoU [21] to compute the success metric, denoted as spherical success S_{sphere} , while only S_{sphere} and P_{angle} are measured.

Evaluation on segmentation. Region similarity \mathcal{J} and contour accuracy \mathcal{F} [42] are two common metrics in evaluation of segmentation results. Region similarity \mathcal{J} measures the pixel-based IoU between an output segmentation M^{tr} and its ground truth mask M^{gt} . \mathcal{F} computes the F1-score by precision and recall on contour P^c and R^c between the contours of M^{tr} and M^{gt} . The two standard metrics are defined as:

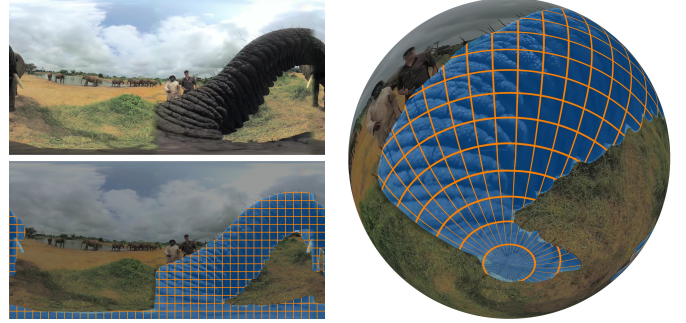
$$\mathcal{J} = IoU(M^{gt}, M^{tr}), \quad \mathcal{F} = \frac{2P^cR^c}{P^c + R^c}. \quad (12)$$

When a target is situated in high-latitude areas (i.e., close to the top or bottom) on 360° images, its segmentation is usually stretched due to the spherical distortion, leading to issues of overestimation in the metrics of \mathcal{J} and \mathcal{F} . Figure 7a shows a sample target of the mentioned case, as well as its mask and pixel grids in the perspective view (i.e., parallel with the 360° image boundaries) are marked separately. To handle this issue, we re-project the 360° image on a 3D sphere as shown in Figure 7b. The spherical pixel grids near the polar regions contribute less weight to the segmentation than other regions. Considering the weights varying along the latitude, we apply pre-computed spherical weights \mathfrak{W} on the standard metrics \mathcal{J} and \mathcal{F} obtaining two spherical metrics, i.e., spherical region similarity \mathcal{J}_{sphere} and spherical contour accuracy \mathcal{F}_{sphere} .

Specifically, in a 360° image with width W and height H , the spherical weight measuring the importance of a specific pixel $[u, v]$ can be defined by the corresponding surface area on a unit sphere (radius $r = 1$), formulated as:

$$\mathfrak{W}_{u,v} = \left\| \int_{\varphi-\Delta\varphi/2}^{\varphi+\Delta\varphi/2} \int_{\vartheta-\Delta\vartheta/2}^{\vartheta+\Delta\vartheta/2} \sin \vartheta \, d\vartheta d\varphi \right\|, \quad (13)$$

where $[\vartheta, \varphi]$ is the longitude and latitude of the spherical coordinate which can be computed from $[u, v]$ via Eq. 6, $\Delta\vartheta = \pi/H$ and $\Delta\varphi = 2\pi/W$.



(a) Sample 360° image with a target elephant and its corresponding mask with perspective pixel-grids. (b) Projection of the mask and grids on a spherical surface, where the size of the grids varies with latitude.

Fig. 7: Difference between perspective pixel grids on a 360° image and spherical pixel grids on a 3D sphere.

With the pre-computed spherical weights, spherical region similarity \mathcal{J}_{sphere} is defined by:

$$\mathcal{J}_{sphere} = IoU(M^{gt} \odot \mathfrak{W}, M^{tr} \odot \mathfrak{W}). \quad (14)$$

For evaluating contour accuracy on a sphere \mathcal{F}_{sphere} , we adopt the bipartite graph matching [43] as in [42]. The spherical contour accuracy \mathcal{F}_{sphere} is measured by:

$$\begin{aligned} P_{sphere}^c &= \frac{\sum \Psi(c(M^{tr})|c(M^{gt})) \odot \mathfrak{W}}{\sum c(M^{tr}) \odot \mathfrak{W}}, \\ R_{sphere}^c &= \frac{\sum \Psi(c(M^{gt})|c(M^{tr})) \odot \mathfrak{W}}{\sum c(M^{gt}) \odot \mathfrak{W}}, \\ \mathcal{F}_{sphere} &= \frac{2P_{sphere}^c R_{sphere}^c}{P_{sphere}^c + R_{sphere}^c}, \end{aligned} \quad (15)$$

where the matching operation $\Psi(\cdot|\cdot)$, the contour of a mask $c(\cdot)$, and the element-wise multiplication \odot .

B. VOT Evaluation

VOT baseline trackers. We evaluated 20 state-of-the-art visual object trackers on 360VOT, as shown in Table III. According to the latest development of visual tracking, the compared methods can be roughly classified into three groups: transformer trackers, Siamese trackers, and other deep learning-based trackers. Specifically, the transformer trackers contain Stark [44], ToMP [45], MixFormer [46], SimTrack [47] and AiATrack [48]. The Siamese trackers include SiamDW [49], SiamMask [39], SiamRPNpp [4], SiamBAN [50], AutoMatch [51], Ocean [52] and SiamX [37]. For other deep trackers, UDT [53], Meta-SDNet [54], MD-Net [2], ECO [3], ATOM [55], KYS [56], DiMP [5], PrDiMP [57] were evaluated. We used the official implementation, trained models, and default configurations to ensure a fair comparison among trackers. In addition, we developed a new baseline AiATrack-360 that combines the transformer tracker AiATrack [48] with our 360 tracking framework. We also adapted a different kind of tracker SiamX [37] with our framework, named SiamX-360, to verify the generality of the proposed framework.

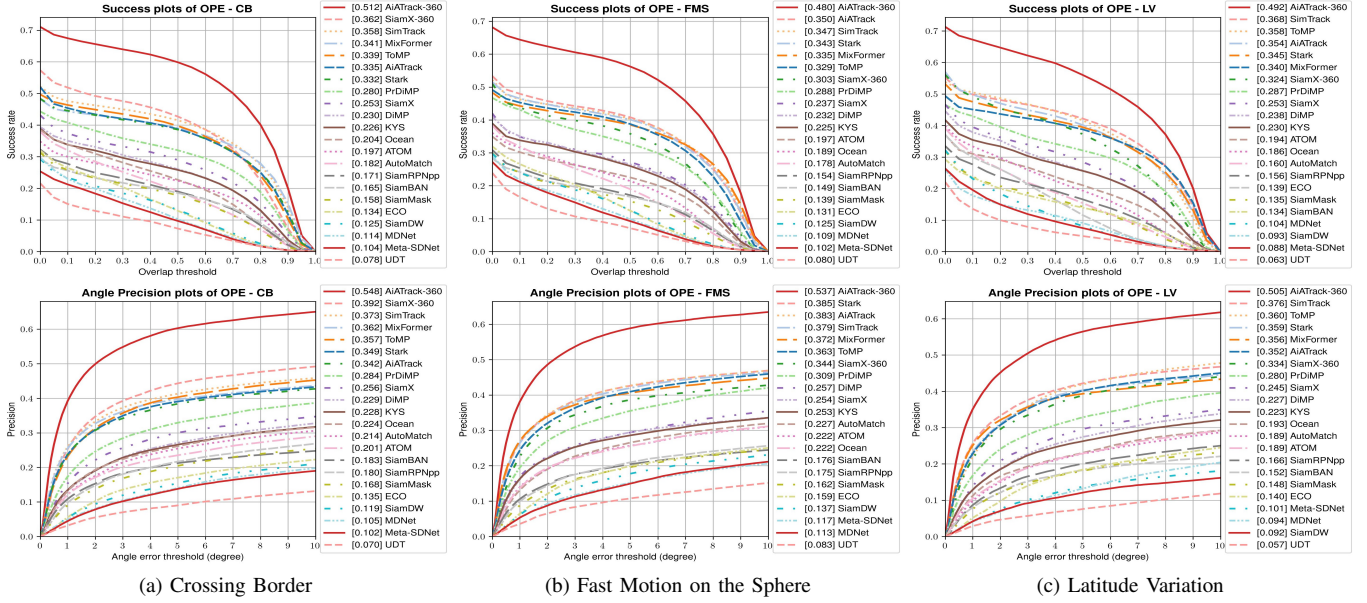


Fig. 8: Comparing BBox tracking performances in 360VOT of different trackers, in terms of dual success rate and angle precision rate under the three distinct attributes of 360VOT.

TABLE III

Overall performance on 360VOT BBox in terms of dual success, dual precision, dual normalized precision, and angle precision. Bold blue indicates the best results in the tracker group. Bold red indicates the best results overall.

VOT Tracker	360VOT BBox			
	S_{dual} (AUC)	P_{dual}	\bar{P}_{dual} (AUC)	P_{angle}
UDT [53]	0.104	0.075	0.117	0.098
Meta-SDNet [54]	0.131	0.097	0.164	0.136
MDNet [2]	0.150	0.106	0.188	0.143
ECO [3]	0.175	0.130	0.212	0.179
ATOM [55]	0.252	0.216	0.286	0.266
KYS [56]	0.286	0.245	0.312	0.296
DiMP [5]	0.290	0.247	0.315	0.299
PrDiMP [57]	0.341	0.292	0.371	0.347
SiamDW [49]	0.156	0.116	0.190	0.156
SiamMask [39]	0.189	0.161	0.220	0.203
SiamRPNpp [4]	0.201	0.175	0.233	0.213
SiamBAN [50]	0.205	0.187	0.242	0.227
AutoMatch [51]	0.208	0.202	0.261	0.248
Ocean [52]	0.240	0.223	0.287	0.264
SiamX [37]	0.302	0.265	0.331	0.315
Stark [44]	0.381	0.356	0.403	0.408
ToMP [45]	0.393	0.352	0.421	0.413
MixFormer [46]	0.395	0.378	0.417	0.424
SimTrack [47]	0.400	0.373	0.421	0.424
AiATrack [48]	0.405	0.369	0.427	0.423
SiamX-360	0.391	0.365	0.430	0.425
AiATrack-360	0.534	0.506	0.563	0.574

Overall performance on BBox. Existing trackers take the BBox of the first frame to initialize the tracking, and the inference results are also in the form of BBox. Table III shows comparison results among four groups of trackers, i.e., other, Siamese, transformer baselines, and the adapted trackers for each block in the table. According to the quantitative results, PrDiMP [57], SiamX [37] and AiATrack-360 perform best in their group of trackers. Owing to the powerful network archi-

TABLE IV

Tracking performance based on other annotations of 360VOT using 360 tracking framework.

VOT Tracker	360VOT rBBox			
	S_{dual} (AUC)	P_{dual}	\bar{P}_{dual} (AUC)	P_{angle}
SiamX-360	0.205	0.278	0.278	0.327
AiATrack-360	0.362	0.449	0.516	0.535
	360VOT BFoV		360VOT rBFoV	
	S_{sphere} (AUC)	P_{angle}	S_{sphere} (AUC)	P_{angle}
SiamX-360	0.262	0.327	0.243	0.323
AiATrack-360	0.548	0.564	0.426	0.530

tectures, the *transformer* trackers generally outperform other groups of the compared trackers. After AiATrack integrates our proposed framework, AiATrack-360 achieves a significant performance increase of 12.9%, 13.7%, 13.6% and 15.1% in terms of S_{dual} , P_{dual} , \bar{P}_{dual} and P_{angle} respectively. AiATrack-360 outperforms all other trackers with a big performance gap. Compared to SiamX, SiamX-360 is improved by 8.9% S_{dual} , 10% P_{dual} , 9.6% \bar{P}_{dual} and 11% P_{angle} , which is comparable with other transformer trackers. Although the performance gains of AiATrack-360 and SiamX-360 are different, the difference validates the effectiveness and generalization of our 360 tracking framework on 360° visual object tracking. They can serve as a new baseline for future comparison.

Attribute-based performance on BBox. Furthermore, we evaluated all trackers under 20 attributes to analyze different challenges. In Figure 8, we plot the results on the videos with cross border (CB), fast motion on the sphere (FMS), and latitude variation (LV) attributes. These are the three exclusive and most challenging attributes of 360VOT. Compared to the overall performance, all trackers suffer performance degradation, especially on the CB and FMS attributes. For example, P_{dual} of SimTrack decreases by 4.2% and 5.3% on CB and

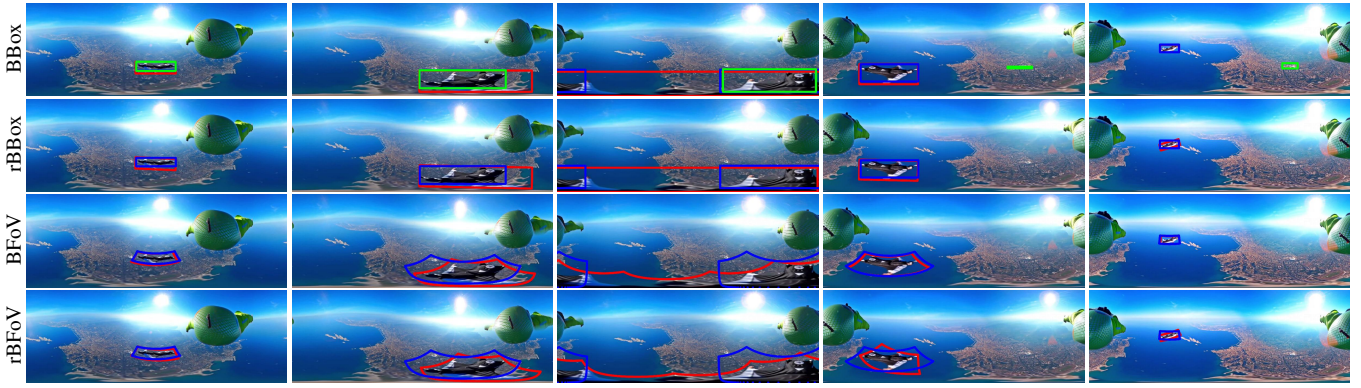


Fig. 9: Qualitative tracking results of the baseline on different representations of 360VOT. Red denotes the ground truth, and blue denotes the results of AiATrack-360. The green in the first row denotes the results of AiATrack.

FMS respectively. However, the performance of AiATrack-360 still dominates on all three adverse attributes, while SiamX-360 also obtains stable performance gains.

Performance based on other annotations. Apart from BBox, we provide additional ground truth, including rBBox and (r)BFoV. As our 360 tracking framework can estimate approximate rBBox and (r)BFoV from local BBox predictions, we additionally evaluate the performances of SiamX-360 and AiATrack-360 on these three representations (Table IV). Compared with the results on BBox (Table III), the performance on rBBox declines vastly. SiamX-360 and AiATrack-360 only achieve 0.205 and 0.362 S_{dual} respectively. By contrast, the evaluation of (r)BFoV has more reasonable and consistent numbers. In addition, we display visual results by AiATrack-360 and AiAtrack in Figure 9. AiATrack-360 can follow and localize targets in challenging cases. Compared with (r)BBox, (r)BFoV can bind targets accurately with fewer irrelevant areas. From the extensive evaluation, we observe that (r)BFoV is beneficial for object localization in omnidirectional scenes.

C. VOS Evaluation

VOS baseline trackers. On 360VOS benchmark, we tested 16 state-of-the-art video object segmentation trackers. Among them, we included five memory-based methods that have demonstrated impressive results in VOS tasks: STM [6], GMVOS [58], STCN [59], XMem [10], and XMem++ [60]. Additionally, we evaluated unified VOS methods across segmentation and tracking namely RTS [38], UNICORN [7], and TarViS [61], transformer-based methods including AOT [62] and DeAOT [9], and other learning-based methods including AFB-URR [63], CFBI [8], CFBI+ [64], LWL [65], TBD [66], and JOINT [67]. In the experiments, some listed trackers had excessive GPU and RAM demands when handling a long sequence (i.e., 2400 frames) of 360VOS. For memory-based trackers STCN [59], GMVOS [58], and STM [6], we limited their memory clip length to 16. As for trackers AOT [62] and DeAOT [9] that integrate long-term memory, we only kept the latest 32 clips of their long-term memory. Furthermore, we combined XMem [10] with our 360 tracking framework as a *framework baseline* XMem-360. To verify the efficacy of the 360VOS training set, we retrained XMem [10] to obtain a *retrained baseline* XMem* and evaluated it without our

TABLE V
Segmentation performance on 360VOS in terms of standard and spherical region similarity and contour accuracy. Bold blue indicates the best results in existing trackers, while bold red indicates the best results overall.

VOS Tracker	360VOS			
	\mathcal{J}	\mathcal{F}	\mathcal{J}_{sphere}	\mathcal{F}_{sphere}
STM [6]	0.364	0.438	0.351	0.426
UNICORN [7]	0.339	0.469	0.328	0.461
TarVis [61]	0.325	0.411	0.320	0.407
AFB-URR [63]	0.389	0.481	0.375	0.472
GMVOS [58]	0.431	0.522	0.416	0.508
CFBI [8]	0.412	0.513	0.397	0.502
CFBI+ [64]	0.428	0.532	0.414	0.525
DeAOT [9]	0.447	0.578	0.433	0.569
AOT [62]	0.471	0.597	0.457	0.589
LWL [65]	0.469	0.567	0.457	0.559
TBD [66]	0.474	0.598	0.459	0.590
JOINT [67]	0.487	0.587	0.476	0.581
RTS [38]	0.540	0.645	0.530	0.641
STCN [59]	0.550	0.667	0.535	0.657
XMem [10]	0.560	0.662	0.550	0.659
XMem++ [60]	0.579	0.692	0.570	0.687
Xmem*	0.596	0.703	0.584	0.699
XMem-360	0.656	0.780	0.639	0.771
XMem-360*	0.665	0.786	0.651	0.779

framework. Finally, we applied the retrained model to the 360 tracking framework, denoted as XMem-360*.

Training details of XMem*. We adhered to a similar training scheme of the original XMem [10] to retrain the weights of the XMem network. We first utilized its initialized weights that were pre-trained on static images and BL30K dataset [68], and then we directly performed the main training stage on the combination of our 360VOS training set, YouTubeVOS [19] and DAVIS [18]. To reduce memory cost while learning details on the high-resolution 360° images of 360VOS, we downsampled each frame from 4K resolution to 720p (i.e., 1440×720) for training. During training, all training frames were randomly cropped to 512 × 512. We employed bootstrapped cross entropy loss and dice loss functions to optimize the model. The optimizer we used is AdamW while the learning rate is set to 1e-5 with a weight decay rate of 0.05. The retraining process lasted around 3.5 days, involving 100K iterations with a batch size of 8 on 4 RTX3090 GPUs.

Performance on 360VOS. In each testing sequence, the mask



Fig. 10: Comparison between the ground truth (GT) and the results from XMem [10] and our three new baselines. The output **masks** and **BFoVs** are shown with distinct colors. The 360 tracking framework enhances performance in addressing specific challenges, such as crossing border (CB) and large distortion (LD), while the retraining strategy (i.e. XMem*, XMem-360*) yields noticeable improvements on large distortion and stitching artifact (SA).

was initialized on the first frame, and all trackers subsequently inferred masks for the following frames. According to the quantitative results reported in Table V, memory-based methods such as STCN [59], XMem [10], and XMem++ [60] outperform other existing trackers when dealing with omnidirectional scenes. Particularly, XMem++ [60] achieve the top performance among the 16 existing trackers, with scores of 0.579, 0.692, 0.570, and 0.687 in terms of \mathcal{J} , \mathcal{F} , $\mathcal{J}_{\text{sphere}}$, and $\mathcal{F}_{\text{sphere}}$, respectively. By leveraging the 360VOS data knowledge, the *retrained baseline* XMem* still show a noticeable improvement of 1.7%, 1.1%, 1.4%, and 1.2% compared to XMem++ [60] in terms of \mathcal{J} , \mathcal{F} , $\mathcal{J}_{\text{sphere}}$, and $\mathcal{F}_{\text{sphere}}$. With our proposed framework, both XMem-360 and XMem-360* demonstrate significant improvements over all other trackers. Notably, XMem-360* and XMem* achieve slightly better performance than XMem-360 and XMem, respectively, which present the effectiveness of the 360VOS training set in addressing the intricate appearance variance of tracking targets in 360VOS tasks, as exemplified in Figure 10.

Tracking performance of VOS trackers on 360VOT. To explore the potential for cross-domain methodological enhancements that integrate the strength of VOS and VOT methods, we conducted additional experiments to evaluate the tracking performance of VOS trackers on the 360VOT benchmark. In the implementation, we converted the VOS outputs of XMem [10] and the 3 new baselines to obtain the tracking results in terms of (r)BBox and (r)BFoV. The comparisons with the pure VOT trackers (i.e., AiATrack-360 and SiamX-360) are demonstrated in Table VI. XMem [10] exhibits commendable performance in VOT tasks surpassing SiamX-360. Compared to AiATrack-360, XMem-360 shows comparable performance while the tracking precision is higher. For example, the rBBox angle precision P_{angle} of XMem-360 outperforms AiATrack-360 by 3.9%. It indicates an outstanding capability of VOS trackers in handling objects with complex orientations within

TABLE VI

Tracking performance of adapting VOS trackers on the 360VOT benchmark. (VOT) indicates the (r)BBox and (r)BFoV results of the trackers are converted from their original output masks. In the same group of performance, bold **red** highlights the best results, while bold **blue** highlights the second results.

Tracker	360VOT BBox			
	$S_{\text{dual}}(\text{AUC})$	P_{dual}	$\bar{P}_{\text{dual}}(\text{AUC})$	P_{angle}
SiamX-360	0.391	0.365	0.430	0.425
AiATrack-360	0.534	0.506	0.563	0.574
(VOT) XMem [10]	0.432	0.425	0.460	0.465
(VOT) XMem*	0.523	0.529	0.553	0.576
(VOT) XMem-360	0.535	0.534	0.566	0.588
(VOT) XMem-360*	0.583	0.588	0.607	0.637
Tracker	360VOT rBBox			
	$S_{\text{dual}}(\text{AUC})$	P_{dual}	$\bar{P}_{\text{dual}}(\text{AUC})$	P_{angle}
SiamX-360	0.205	0.278	0.278	0.327
AiATrack-360	0.362	0.449	0.516	0.535
(VOT) XMem [10]	0.288	0.411	0.430	0.457
(VOT) XMem*	0.347	0.511	0.517	0.564
(VOT) XMem-360	0.357	0.512	0.524	0.574
(VOT) XMem-360*	0.387	0.566	0.565	0.624
Tracker	360VOT BFoV		360VOT rBFoV	
	$S_{\text{sphere}}(\text{AUC})$	P_{angle}	$S_{\text{sphere}}(\text{AUC})$	P_{angle}
SiamX-360	0.262	0.327	0.243	0.323
AiATrack-360	0.548	0.564	0.426	0.530
(VOT) XMem [10]	0.435	0.465	0.414	0.458
(VOT) XMem*	0.523	0.575	0.498	0.568
(VOT) XMem-360	0.541	0.585	0.514	0.577
(VOT) XMem-360*	0.594	0.635	0.565	0.626

360° videos. This is further evidenced by an obvious performance gain in the rBFoV evaluation. Moreover, XMem-360* achieves consistent advancements across all tracking metrics, proving the effectiveness of the training set.

VI. DISCUSSION AND CONCLUSION

In this paper, we explore omnidirectional visual object tracking and segmentation. We take advantage of BFoV to represent target positions on 360° images and extract less-distorted searching regions. The BFoV representation thus becomes the wheel in our 360 tracking framework that can adopt arbitrary classical local visual trackers to perform visual object tracking or segmentation in omnidirectional videos. The integration of existing algorithms into our 360 tracking framework demonstrates promising results in handling the intricate challenges posed by spherical distortions on 360° images. In addition, we introduced a comprehensive benchmark dataset 360VOTS designed to facilitate the study of both omnidirectional visual object tracking and segmentation. The newly available training data also provides an effective way to enhance the tracker’s performance.

Nevertheless, there still remains a big room for improvement and we want to discuss some promising directions here. One of them is the development of long-term omnidirectional tracking algorithms. The trackers enhanced by our tracking framework are still classified as short-term trackers technically. As target occlusion is a noticeable attribute of 360VOTS, the long-term tracker capable of target relocalization can perform better. However, how to effectively and efficiently search for targets on the whole 360° image is a challenge. Another promising direction is exploring new network architectures. The trackers exploiting network architectures [69], [70] tailored for omnidirectional images may be able to extract better features and correlations for robust VOT and VOS.

By introducing new representations, new datasets, new metrics, and new benchmarks, we envisage 360VOTS will not only catalyze further research on omnidirectional visual object tracking and segmentation but also promote new applications across a broad spectrum of computer vision and robotics fields.

REFERENCES

- [1] J. F. Henriques, R. Caseiro, P. Martins, and J. Batista, “High-speed tracking with kernelized correlation filters,” *TPAMI*, vol. 37, no. 3, pp. 583–596, 2014. [1](#)
- [2] H. Nam and B. Han, “Learning multi-domain convolutional neural networks for visual tracking,” in *CVPR*, 2016. [1](#), [7](#), [8](#)
- [3] M. Danelljan, G. Bhat, F. Shahbaz Khan, and M. Felsberg, “Eco: Efficient convolution operators for tracking,” in *CVPR*, 2017, pp. 6638–6646. [1](#), [7](#), [8](#)
- [4] B. Li, W. Wu, Q. Wang, F. Zhang, J. Xing, and J. Yan, “Siamrpn++: Evolution of siamese visual tracking with very deep networks,” in *CVPR*, 2019, pp. 4282–4291. [1](#), [7](#), [8](#)
- [5] G. Bhat, M. Danelljan, L. V. Gool, and R. Timofte, “Learning discriminative model prediction for tracking,” in *ICCV*, 2019, pp. 6182–6191. [1](#), [7](#), [8](#)
- [6] S. W. Oh, J.-Y. Lee, N. Xu, and S. J. Kim, “Video object segmentation using space-time memory networks,” in *ICCV*, 2019. [1](#), [9](#)
- [7] B. Yan, Y. Jiang, P. Sun, D. Wang, Z. Yuan, P. Luo, and H. Lu, “Towards grand unification of object tracking,” in *ECCV*, vol. 13681, 2022, pp. 733–751. [1](#), [9](#)
- [8] Z. Yang, Y. Wei, and Y. Yang, “Collaborative video object segmentation by foreground-background integration,” in *ECCV*, vol. 12350, 2020, pp. 332–348. [1](#), [9](#)
- [9] Z. Yang and Y. Yang, “Decoupling features in hierarchical propagation for video object segmentation,” in *NeurIPS*, vol. 35, 2022, pp. 36324–36336. [1](#), [9](#)
- [10] H. K. Cheng and A. G. Schwing, “Xmem: Long-term video object segmentation with an atkinson-shiffrin memory model,” in *ECCV*, vol. 13688, 2022, pp. 640–658. [1](#), [9](#), [10](#)
- [11] Y. Wu, J. Lim, and M.-H. Yang, “Object tracking benchmark,” *TPAMI*, vol. 37, no. 9, pp. 1834–1848, 2015. [1](#), [2](#), [3](#), [6](#)
- [12] M. Mueller, N. Smith, and B. Ghanem, “A benchmark and simulator for uav tracking,” in *ECCV*, 2016, pp. 445–461. [1](#), [2](#), [3](#)
- [13] M. Kristan, J. Matas, A. Leonardis, T. Vojir, R. Pflugfelder, G. Fernandez, G. Nebehay, F. Porikli, and L. Čehovin, “A novel performance evaluation methodology for single-target trackers,” *TPAMI*, vol. 38, no. 11, pp. 2137–2155, Nov 2016. [1](#), [2](#), [3](#)
- [14] H. Fan, L. Lin, F. Yang, P. Chu, G. Deng, S. Yu, H. Bai, Y. Xu, C. Liao, and H. Ling, “Lasot: A high-quality benchmark for large-scale single object tracking,” in *CVPR*, 2019, pp. 5374–5383. [1](#), [2](#), [3](#)
- [15] L. Huang, X. Zhao, and K. Huang, “Got-10k: A large high-diversity benchmark for generic object tracking in the wild,” *TPAMI*, vol. 43, no. 5, pp. 1562–1577, 2019. [1](#), [2](#), [3](#)
- [16] P. Ochs, J. Malik, and T. Brox, “Segmentation of moving objects by long term video analysis,” *TPAMI*, vol. 36, no. 6, pp. 1187 – 1200, Jun 2014, preprint. [1](#), [2](#), [3](#)
- [17] L. Hong, W. Chen, Z. Liu, W. Zhang, P. Guo, Z. Chen, and W. Zhang, “Lvos: A benchmark for long-term video object segmentation,” in *ICCV*, 2023, pp. 13480–13492. [1](#), [3](#)
- [18] J. Pont-Tuset, F. Perazzi, S. Caelles, P. Arbeláez, A. Sorkine-Hornung, and L. Van Gool, “The 2017 davis challenge on video object segmentation,” *arXiv:1704.00675*, 2017. [1](#), [2](#), [3](#), [9](#)
- [19] N. Xu, L. Yang, Y. Fan, D. Yue, Y. Liang, J. Yang, and T. S. Huang, “Youtube-vos: A large-scale video object segmentation benchmark,” *CoRR*, vol. abs/1809.03327, 2018. [1](#), [3](#), [9](#)
- [20] J. P. Snyder, *Flattening the earth: two thousand years of map projections*. University of Chicago Press, 1997. [1](#)
- [21] F. Dai, B. Chen, H. Xu, Y. Ma, X. Li, B. Feng, P. Yuan, C. Yan, and Q. Zhao, “Unbiased iou for spherical image object detection,” in *AAAI*, vol. 36, 2022, pp. 508–515. [1](#), [7](#)
- [22] H. Xu, Q. Zhao, Y. Ma, X. Li, P. Yuan, B. Feng, C. Yan, and F. Dai, “Pandora: A panoramic detection dataset for object with orientation,” in *ECCV*, 2022. [1](#), [3](#), [4](#)
- [23] H. Huang, Y. Xu, Y. Chen, and S.-K. Yeung, “360vot: A new benchmark dataset for omnidirectional visual object tracking,” in *ICCV*, 2023. [1](#), [3](#), [5](#)
- [24] A. W. Smeulders, D. M. Chu, R. Cucchiara, S. Calderara, A. Dehghan, and M. Shah, “Visual tracking: An experimental survey,” *TPAMI*, vol. 36, no. 7, pp. 1442–1468, 2013. [2](#), [3](#)
- [25] A. Li, M. Lin, Y. Wu, M.-H. Yang, and S. Yan, “Nus-pro: A new visual tracking challenge,” *TPAMI*, vol. 38, no. 2, pp. 335–349, 2015. [2](#), [3](#)
- [26] P. Liang, E. Blasch, and H. Ling, “Encoding color information for visual tracking: Algorithms and benchmark,” *IEEE transactions on image processing*, vol. 24, no. 12, pp. 5630–5644, 2015. [2](#), [3](#)
- [27] S. Li and D.-Y. Yeung, “Visual object tracking for unmanned aerial vehicles: A benchmark and new motion models,” in *AAAI*, vol. 31, 2017. [2](#), [3](#)
- [28] H. Kiani Galoogahi, A. Fagg, C. Huang, D. Ramanan, and S. Lucey, “Need for speed: A benchmark for higher frame rate object tracking,” in *ICCV*, 2017, pp. 1125–1134. [2](#), [3](#)
- [29] D. Du, Y. Qi, H. Yu, Y. Yang, K. Duan, G. Li, W. Zhang, Q. Huang, and Q. Tian, “The unmanned aerial vehicle benchmark: Object detection and tracking,” in *ECCV*, 2018, pp. 370–386. [2](#), [3](#)
- [30] J. Valmadre, L. Bertinetto, J. F. Henriques, R. Tao, A. Vedaldi, A. W. Smeulders, P. H. Torr, and E. Gavves, “Long-term tracking in the wild: A benchmark,” in *ECCV*, 2018, pp. 670–685. [2](#), [3](#)
- [31] M. Muller, A. Bibi, S. Giancola, S. Alsubaihi, and B. Ghanem, “Trackingnet: A large-scale dataset and benchmark for object tracking in the wild,” in *ECCV*, 2018, pp. 300–317. [2](#), [3](#), [6](#)
- [32] H. Fan, H. A. Miththanathaya, S. R. Rajan, X. Liu, Z. Zou, Y. Lin, H. Ling *et al.*, “Transparent object tracking benchmark,” in *ICCV*, 2021, pp. 10734–10743. [2](#), [3](#)
- [33] M. Dunnhofer, A. Furnari, G. M. Farinella, and C. Micheloni, “Is first person vision challenging for object tracking?” in *ICCV*, 2021, pp. 2698–2710. [2](#), [3](#)
- [34] E. Real, J. Shlens, S. Mazzocchi, X. Pan, and V. Vanhoucke, “Youtube-boundingboxes: A large high-precision human-annotated data set for object detection in video,” in *CVPR*, 2017, pp. 5296–5305. [2](#)
- [35] Y. Wu, J. Lim, and M.-H. Yang, “Online object tracking: A benchmark,” in *CVPR*, 2013, pp. 2411–2418. [2](#)
- [36] Z. Zhu, Q. Wang, B. Li, W. Wu, J. Yan, and W. Hu, “Distractor-aware siamese networks for visual object tracking,” in *ECCV*, 2018, pp. 101–117. [3](#)
- [37] H. Huang and S.-K. Yeung, “Siamx: An efficient long-term tracker using cross-level feature correlation and adaptive tracking scheme,” in *ICRA*, 2022. [3](#), [7](#), [8](#)

- [38] M. Paul, M. Danelljan, C. Mayer, and L. V. Gool, “Robust visual tracking by segmentation,” in *ECCV*, vol. 13682, 2022, pp. 571–588. 3, 9
- [39] Q. Wang, L. Zhang, L. Bertinetto, W. Hu, and P. H. Torr, “Fast online object tracking and segmentation: A unifying approach,” in *CVPR*, 2019, pp. 1328–1338. 3, 7, 8
- [40] P. Zhao, A. You, Y. Zhang, J. Liu, K. Bian, and Y. Tong, “Spherical criteria for fast and accurate 360° object detection,” *AAAI*, vol. 34, no. 07, p. 12959–12966, 2020. 3, 4
- [41] H. Huang and S.-K. Yeung, “360vo: Visual odometry using a single 360 camera,” in *ICRA*, 2022, pp. 5594–5600. 4
- [42] F. Perazzi, J. Pont-Tuset, B. McWilliams, L. Van Gool, M. Gross, and A. Sorkine-Hornung, “A benchmark dataset and evaluation methodology for video object segmentation,” in *CVPR*, 2016. 7
- [43] D. Martin, C. Fowlkes, and J. Malik, “Learning to detect natural image boundaries using local brightness, color, and texture cues,” *TPAMI*, vol. 26, no. 5, pp. 530–549, 2004. 7
- [44] B. Yan, H. Peng, J. Fu, D. Wang, and H. Lu, “Learning spatio-temporal transformer for visual tracking,” in *ICCV*, 2021, pp. 10448–10457. 7, 8
- [45] C. Mayer, M. Danelljan, G. Bhat, M. Paul, D. P. Paudel, F. Yu, and L. Van Gool, “Transforming model prediction for tracking,” in *CVPR*, 2022, pp. 8731–8740. 7, 8
- [46] Y. Cui, C. Jiang, L. Wang, and G. Wu, “Mixformer: End-to-end tracking with iterative mixed attention,” in *CVPR*, 2022, pp. 13608–13618. 7, 8
- [47] B. Chen, P. Li, L. Bai, L. Qiao, Q. Shen, B. Li, W. Gan, W. Wu, and W. Ouyang, “Backbone is all your need: A simplified architecture for visual object tracking,” *arXiv preprint arXiv:2203.05328*, 2022. 7, 8
- [48] S. Gao, C. Zhou, C. Ma, X. Wang, and J. Yuan, “Aiatrack: Attention in attention for transformer visual tracking,” in *ECCV*, 2022, pp. 146–164. 7, 8
- [49] Z. Zhang and H. Peng, “Deeper and wider siamese networks for real-time visual tracking,” in *CVPR*, June 2019. 7, 8
- [50] Z. Chen, B. Zhong, G. Li, S. Zhang, and R. Ji, “Siamese box adaptive network for visual tracking,” in *CVPR*, 2020, pp. 6668–6677. 7, 8
- [51] Z. Zhang, Y. Liu, X. Wang, B. Li, and W. Hu, “Learn to match: Automatic matching network design for visual tracking,” in *CVPR*, 2021, pp. 13339–13348. 7, 8
- [52] Z. Zhang, H. Peng, J. Fu, B. Li, and W. Hu, “Ocean: Object-aware anchor-free tracking,” in *ECCV*, 2020, pp. 771–787. 7, 8
- [53] N. Wang, Y. Song, C. Ma, W. Zhou, W. Liu, and H. Li, “Unsupervised deep tracking,” in *CVPR*, 2019. 7, 8
- [54] E. Park and A. C. Berg, “Meta-tracker: Fast and robust online adaptation for visual object trackers,” in *ECCV*, 2018, pp. 569–585. 7, 8
- [55] M. Danelljan, G. Bhat, F. S. Khan, and M. Felsberg, “Atom: Accurate tracking by overlap maximization,” in *CVPR*, 2019, pp. 4660–4669. 7, 8
- [56] G. Bhat, M. Danelljan, L. Van Gool, and R. Timofte, “Know your surroundings: Exploiting scene information for object tracking,” in *ECCV*, 2020, pp. 205–221. 7, 8
- [57] M. Danelljan, L. V. Gool, and R. Timofte, “Probabilistic regression for visual tracking,” in *CVPR*, 2020, pp. 7183–7192. 7, 8
- [58] X. Lu, W. Wang, M. Danelljan, T. Zhou, J. Shen, and L. V. Gool, “Video object segmentation with episodic graph memory networks,” in *ECCV*, vol. 12348, 2020, pp. 661–679. 9
- [59] H. K. Cheng, Y.-W. Tai, and C.-K. Tang, “Rethinking space-time networks with improved memory coverage for efficient video object segmentation,” in *NeurIPS*, vol. 34, 2021, pp. 11781–11794. 9, 10
- [60] M. Bekuzarov, A. Bermudez, J.-Y. Lee, and H. Li, “Xmem++: Production-level video segmentation from few annotated frames,” in *ICCV*, October 2023, pp. 635–644. 9, 10
- [61] A. Athar, A. Hermans, J. Luiten, D. Ramanan, and B. Leibe, “Taris: A unified approach for target-based video segmentation,” in *CVPR*, June 2023, pp. 18738–18748. 9
- [62] Z. Yang, Y. Wei, and Y. Yang, “Associating objects with transformers for video object segmentation,” in *NeurIPS*, vol. 34, 2021, pp. 2491–2502. 9
- [63] Y. Liang, X. Li, N. Jafari, and J. Chen, “Video object segmentation with adaptive feature bank and uncertain-region refinement,” in *NeurIPS*, vol. 33, 2020, pp. 3430–3441. 9
- [64] Z. Yang, Y. Wei, and Y. Yang, “Collaborative video object segmentation by multi-scale foreground-background integration,” *TPAMI*, vol. 44, no. 9, pp. 4701–4712, 2021. 9
- [65] G. Bhat, F. J. Lawin, M. Danelljan, A. Robinson, M. Felsberg, L. V. Gool, and R. Timofte, “Learning what to learn for video object segmentation,” in *ECCV*, vol. 12347, 2020, pp. 777–794. 9
- [66] S. Cho, H. Lee, M. Lee, C. Park, S. Jang, M. Kim, and S. Lee, “Tackling background distraction in video object segmentation,” in *ECCV*, vol. 13682, 2022, pp. 446–462. 9
- [67] Y. Mao, N. Wang, W. Zhou, and H. Li, “Joint inductive and transductive learning for video object segmentation,” in *ICCV*, 2021, pp. 9670–9679. 9
- [68] H. K. Cheng, Y.-W. Tai, and C.-K. Tang, “Modular interactive video object segmentation: Interaction-to-mask, propagation and difference-aware fusion,” in *CVPR*, 2021. 9
- [69] B. Coors, A. P. Condurache, and A. Geiger, “Spherenet: Learning spherical representations for detection and classification in omnidirectional images,” in *ECCV*, 2018, pp. 518–533. 11
- [70] M. Defferrard, M. Milani, F. Gusset, and N. Perraudin, “DeepSphere: a graph-based spherical cnn,” *arXiv preprint arXiv:2012.15000*, 2020. 11



Yinzhe Xu received the B.S. degree in Integrative Systems and Design from the Hong Kong University of Science and Technology. He is currently working toward the Ph.D. degree at the same university. His research interests include omnidirectional vision, object tracking and segmentation, and SLAM.



Huajian Huang obtained his Ph.D. degree in Computer Science and Engineering at the Hong Kong University of Science and Technology. Before the PhD, He received his B.Eng at the Sun Yat-Sen University, China. His research focuses on omnidirectional perception, visual localization, mapping, SLAM, and 3D vision.



Yingshu Chen received the B.Eng in Digital Media Technology from Zhejiang University, and M.Sc in Computer Science from The University of Hong Kong. She is currently a Ph.D. candidate in the Department of Computer Science and Engineering, the Hong Kong University of Science and Technology. Her research interests cover computer vision and computer graphics for computational design such as 2D and 3D style transfer.



Sai-Kit Yeung is currently an Associate Professor at the Division of Integrative Systems and Design, the Department of Computer Science and Engineering, and the Department of Ocean Science at the Hong Kong University of Science and Technology (HKUST). Before joining HKUST, he was an Assistant Professor at the Singapore University of Technology and Design (SUTD) and founded the Vision, Graphics and Computational Design (VGD) Group. During his time at SUTD, he was also a Visiting Assistant Professor at the Computer Science Department at Stanford University and the Computer Science and Artificial Intelligence Laboratory at MIT. Prior to that, he had been a Postdoctoral Scholar in the Department of Mathematics, the University of California, Los Angeles (UCLA). He received his Ph.D. degree in Electronic and Computer Engineering, M.Phil. degree in Bioengineering, and B.Eng. degree (First Class Honors) from HKUST, respectively in 2009, 2005, and 2003.